Midnight latitude-altitude distribution of 630 nm airglow in the Asian sector measured with FORMOSAT-2/ISUAL

Toru Adachi,[1,2] Masashi Yamaoka,[1] Mamoru Yamamoto,[1] Yuichi Otsuka,[3] Huixin Liu,[1] Chun-Chieh Hsiao,[4] Alfred B. Chen,[5] and Rue-Ron Hsu[5]

Received 30 November 2009; revised 6 March 2010; accepted 16 April 2010; published 18 September 2010.

[1] The Imager for Sprites and Upper Atmospheric Lightning (ISUAL) payload on board the FORMOSAT-2 satellite carried out the first limb imaging observation of 630 nm airglow for the purpose of studying physical processes in the *F* region ionosphere. For a total of 14 nights in 2006–2008, ISUAL scanned the midnight latitude-altitude distribution of 630 nm airglow in the Asian sector. On two nights of relatively active conditions (ΣKp = 26, 30+) we found several bright airglow regions, which were highly variable each night in terms of luminosity and location. In relatively quiet conditions (ΣKp = 4–20) near May/June we found two bright regions which were stably located in the midlatitude region of 40°S–10°S (50°S–20°S magnetic latitude (MLAT)) and in the equatorial region of 0°–10°N (10°S–0° MLAT). On one of the quiet nights, FORMOSAT-3/COSMIC and CHAMP simultaneously measured the plasma density in the same region where ISUAL observed airglow. The plasma density data generally show good agreement, suggesting that plasma enhancements were the primary source of these two bright airglow regions. From detailed comparison with past studies we explain that the airglow in the equatorial region was due to the midnight brightness wave produced in association with the midnight temperature maximum, while that in the midlatitude region was due to the typical plasma distribution usually formed in the midnight sector. The fact that the equatorial airglow was much brighter than the midlatitude airglow and was observed on most nights during the campaign period strongly suggests the importance of further studies on the MTM/MBW phenomenology, which is not well reproduced in the current general circulation model.

Citation: Adachi, T., M. Yamaoka, M. Yamamoto, Y. Otsuka, H. Liu, C.-C. Hsiao, A. B. Chen, and R.-R. Hsu (2010), Midnight latitude-altitude distribution of 630 nm airglow in the Asian sector measured with FORMOSAT-2/ISUAL, *J. Geophys. Res.*, *115*, A09315, doi:10.1029/2009JA015147.

1. Introduction

[2] The *F* region ionosphere is controlled by interactions of plasma with neutral particles. Daytime photoionization due to solar ultraviolet radiation drives various chemical reactions that induce several airglows in the ionosphere. The 630 nm airglow, which is the target of our observations, is due to the excited atomic oxygen in the *F* region. Ground-based observation of 630 nm airglow is one of the most powerful methods for elucidating the horizontal structure of the ionosphere. *Barbier and Glaume* [1960], using a scanning photometer deployed on the ground, first found the existence of the tropical arc caused by the equatorial ionospheric anomaly (EIA). Further studies have found various unique phenomena such as large-scale and medium-scale traveling ionospheric disturbances (TIDs) [e.g., *Saito et al.*, 2001; *Shiokawa et al.*, 2003; *Otsuka et al.*, 2004]. Especially in the midnight sector, bright airglow is often observed in the low-latitude region and is referred to as the midnight brightness wave [*Colerico et al.*, 1996]. While past ground-based observations have revealed physical processes occurring in the *F* region ionosphere, they also have some inevitable disadvantages. One of the most distinct weaknesses is a difficulty in obtaining vertical information. As described in section 2, it is clear that the intensity of airglow is sensitive to the *F* region height. Although vertical information is necessary to understand the *F* region ionosphere, it is hard to accurately derive such information from observations at ground level. Another disadvantage is the spatial coverage: because an observation area covered by a ground-based all-sky imager is limited, it is hard to elucidate global behavior of the *F* region ionosphere from the ground.

[1]Research Institute for Sustainable Humanosphere, Kyoto University, Kyoto, Japan.
[2]Now at STAR Laboratory, Stanford University, Stanford, California, USA.
[3]Solar-Terrestrial Environment Laboratory, Nagoya University, Nagoya, Japan.
[4]National Space Organization, Hsin-Chu, Taiwan.
[5]Department of Physics, National Cheng Kung University, Tainan, Taiwan.

0148-0227/10/2009JA015147

[3] So far, several satellite-based limb observations of 630 nm airglow have been carried out to solve these problems. *Chandra et al.* [1973] first analyzed global airglow data obtained by the Ogo 4 satellite. The global map they obtained was asymmetrical with respect to the magnetic equator. On the basis of theoretical expectations that airglow intensity is negatively correlated with altitude, they concluded that the asymmetry resulted from differences in the *F* region height in the north/south hemispheres [e.g., *Reed et al.*, 1973; *Thuilleir and Blamont*, 1973; *Blamont et al.*, 1974]. *Abreu et al.* [1982], analyzing the data from the Visible Airglow Experiment (VAE) on board the Atmosphere Explorer E (AE-E) satellite, derived the altitude profile of 630 nm airglow and suggested the roles of E × B plasma drift and the neutral wind in controlling the structure of the *F* region ionosphere. *Burrage et al.* [1990] also analyzed VAE/AE-E data and estimated the strength of the interhemispheric wind. The result was roughly consistent with model predictions except for the midnight region. *Bhatnagar and Shepherd* [1989] analyzed data obtained from coincident photometric and topside sounding measurements of the ISIS-II spacecraft and found that the seasonal variation of the 630 nm airglow intensity agrees well with that of the *F* region electron density. More recently, *Thuillier et al.* [2002] carried out a comprehensive study using the TIE-GCM simulations and the WIND Imaging Interferometer (WINDII) on board Upper Atmosphere Research Satellite. From WINDII data, they derived the neutral wind speed as well as the 630 nm airglow brightness and found that the airglow intensity was higher in the winter hemisphere because of the summer-to-winter neutral wind.

[4] Although the above past studies have clarified general characteristics of vertical and global airglow distributions, little is known about airglows around the local midnight region where electrodynamical features are unique. One of the most unique features is the midnight brightness wave which is associated with the midnight temperature maximum occurring around the geographic equator. The current general circulation mode fails to accurately reproduce the midnight brightness wave [e.g., *Fesen et al.*, 2002; *Colerico et al.*, 2006] and further extensive studies on the midnight *F* region behavior are required. Recent limb imaging observations by ISUAL on the FORMOSAT-2 satellite uncovered the global distribution of 630 nm airglow in the midnight region. *Rajesh et al.* [2009], analyzing ISUAL-obtained airglow data, discussed the latitudinal distributions of OI and OH airglows. The satellite viewing geometry, however, was not calibrated and true altitude profiles remained unknown. By correcting geometrical effects, the present paper provides the altitude-latitude distribution of airglow in the Asian sector on the basis of the ISUAL airglow data. Comparing them with coincident satellite-based plasma data, we further discuss the neutral and plasma behaviors in the midnight *F* region ionosphere.

2. ISUAL Limb Imaging Observations

[5] The 630 nm airglow is produced by the following chemical reactions.

$$O^+ + O_2 \rightarrow O_2^+ + O \quad (1)$$

$$O_2^+ + e^- \rightarrow O(^1D) + O(^3P, ^1D, ^1S) \quad (2)$$

$$O(^1D) \rightarrow O(^3P) + h\nu(630\text{nm}) \quad (3)$$

These equations represent 630 nm airglow as being produced via charge exchange and dissociative attachment. Given a steady state condition, the intensity of airglow can be expressed by the following equation [*Sobral et al.*, 1993].

$$v_{630} = \frac{0.756 f(^1D) k_5 [O_2][O^+]}{1 + (k_2[N_2] + k_5[O_2] + k_6[e^-] + k_7[O])/A_{1D}} \quad (4)$$

Here, k is the reaction rate coefficient ($k_2 = 2.30 \times 10^{-11}$ cm^{3}s^{-1}, $k_3 = 1.06 \times 10^{-11}$ cm^{3}s^{-1}, $k_5 = 3.20 \times 10^{-11}$ cm^{3}s^{-1}, $k_6 = 6.60 \times 10^{-11}$ cm^{3}s^{-1}, $k_7 = 9.20 \times 10^{-11}$ cm^{3}s^{-1}) and $A_{1D} = 7.45 \times 10^{-3}$ s^{-1} is the Einstein coefficient while $f(^1D) = 1.1$ is the quantum yield. Thus, we see from equation (4) that 630 nm airglow results from both plasma and neutral phenomena in the *F* region ionosphere.

[6] The FORMOSAT-2 (formerly named ROCSAT-2) satellite flies on a sun-synchronous (0930–2130 LT) polar orbit at 891 km and carries a scientific payload named ISUAL (Imager for Sprites and Upper Atmospheric Lightning) [e.g., *Chen et al.*, 2008]. ISUAL consists of an imager deployed with a selectable six color filter wheel, a six color spectrophotometer, and a dual color array photometer, with all fields of view directed toward the midnight (0000 LT) limb [*Chern et al.*, 2003; *Mende et al.*, 2005]. The primary purpose of ISUAL is to observe lightning and transient luminous events (TLEs) such as sprites, elves, blue jets, and gigantic jets [e.g., *Adachi et al.*, 2008]. Therefore, observations of 630 nm airglow were carried out on a special request basis, and the data analyzed in the present paper were obtained during 14 nights in 2006–2008. In order to put the 630 nm airglow layer into the field-of-view (FOV) of ISUAL, the attitude of the satellite was changed from the regular configuration used for lightning/TLE measurements. In this study, a narrowband (628–635 nm) filter for the ISUAL imager was used to cover the atomic oxygen line emission at 630 nm. Since the passband of this filter also covers the OH Meinel band emissions, the images obtained in this work represent the signature of both OI and OH airglow layers, which are located at altitudes of 200–300 km [e.g., *Chandra et al.*, 1973; *Frey et al.* 2001] and 85–90 km [e.g., *Mende et al.*, 1993; *Nikoukar et al.*, 2007], respectively. The FOV of imager is 20 degrees (horizontal: h) × 5 degrees (vertical: v) and the number of pixels is 512 (h) × 128 (v), which corresponds to an area of ~980 km (h) × ~240 km (v) at a spatial resolution of ~1.9 km (both v and h) at the limb located ~2800 km away from the satellite. In our observations, we operated the imager with an exposure time of 0.999 s and a repetition period of 1.004 s. Taking images repeatedly as the satellite moves northward on the orbit, we obtain the latitudinal-altitude distribution of airglow between 25°S and 60°N in the northern winter season and between 40°S and 35°N in the equinox seasons. Since ISUAL scans these latitude ranges in less than 30 min, the macroscopic structure of the airglow does not change significantly. We note that the ISUAL imager data analyzed in the present study is calibrated by laboratory experiments carried out before the launch of the satellite. If we refer to recent orbital calibration results of the ISUAL spectropho-

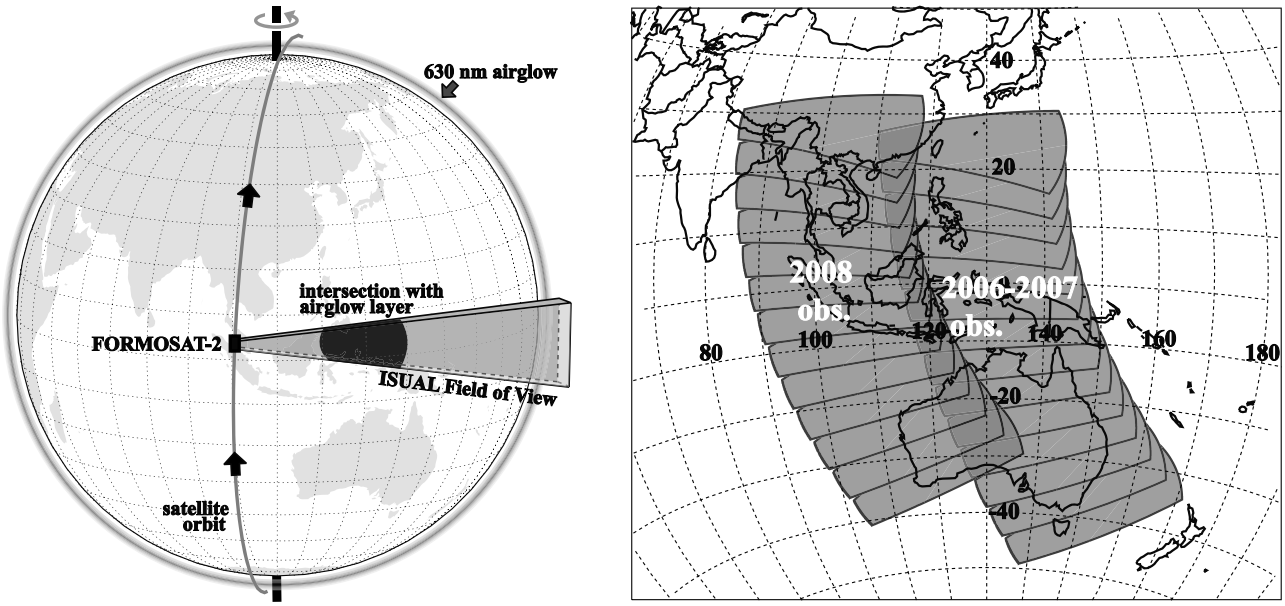

Figure 1. (left) The ISUAL observation geometry and (right) the observed regions projected onto ground. The ISUAL observed 110°E–160°E longitudes in 2006 and 2007 and 90°E–130°E longitudes in 2008.

tometer, the airglow luminosity shown in the present paper would be underestimated to 10–20%. Although the absolute value of luminosity might be underestimated, it does not affect the conclusions about latitude-altitude structure which are the primary contribution of this paper.

[7] Figure 1 shows the geometry of ISUAL airglow observations. The line of sight is directed nearly eastward and the offsets from the true east are smaller at lower latitudes. This offset causes some errors in the positioning of airglow structures and we expect a latitudinal ambiguity of < 10 degrees in the midlatitude region and < 5 degrees in the low-latitude to equatorial region. In this study, ISUAL observed a longitude range of 110°E–160°E on 8 (terrestrial) nights in 2006–2007 and observed a range of 80°E–130°E on 6 nights in 2008. A sample snapshot obtained at 1414:09 (UT) on 20 December 2006 is shown in Figure 2. The upper dim layer is OI airglow in the *F* region ionosphere whereas the lower bright layer is OH airglow in the mesopause region. Here, we need to calibrate the observation geometry to derive true altitude profiles from ISUAL-observed apparent profiles. For simplicity, we assume Gaussian distribution for the true altitude profile.

$$I(z) = I_{\mathrm{p}} \exp\left(-\left(z - z_{\mathrm{p}}\right)^2 / 2\sigma^2\right) \qquad (5)$$

The peak height z_{p}, the maximum intensity I_{p}, and the layer thickness σ are variables. Supposing that the OI airglow layer is horizontally uniform in the ISUAL-viewing (approximately longitudinal) direction, we convert the assumed Gaussian profile into the satellite observation geometry and compare it with the ISUAL-observed apparent profile. This process is iterated over the (z_{p}, I_{p},σ) variable space to find the best fit true profile. Figure 3 shows ISUAL data (solid line) taken from the vertical column at the center of the image shown in Figure 2 and the best fit profile (dotted line) obtained from the iteration process. Here, we used ISUAL data averaged over the 10 horizontal pixels around the center column to reduce pixel noise. The resultant data still has some fluctuations due to the thermal noise of the sensor, which makes an uncertainty of ~0.5 photons cm^{-3} s^{-1} in the airglow volume emission rate. We also examined the sensitivity of the iteration method, changing the values used in the first guess, and found ambiguities of 0.3–0.5 photons cm^{-3} s^{-1}. Therefore, the total error in the observation and analysis process is estimated to be ~1 photons cm^{-3} s^{-1}. It is apparent in Figure 2 that the best fit profile generally agrees well with the ISUAL data. We note that there are some differences, however. The large discrepancy below ~100 km is due to bright OH airglow emissions while that at ~290 km is due to instrumental errors. We excluded these data from comparison in the iteration process. Figure 4 shows the Gaussian distribution of the airglow that best fits the ISUAL-recorded apparent profile shown in Figure 3. Also shown is a typical airglow distribution calculated from the MSIS-E-90 and IRI-2007 empirical models using equation (4). Close matching of these two profiles suggests the validity of this fitting method. Profiles of 630 nm airglow can be well expressed by the Gaussian shape to first

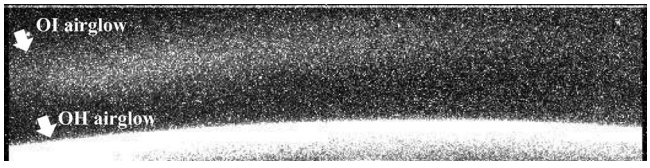

Figure 2. An example of 630 nm imagery observed at 1514:09 UT on 20 December 2006. The upper dim emissions are due to the OI airglow layer in the *F* region ionosphere, while the lower bright emissions are due to the OH airglow layer at around the mesopause.

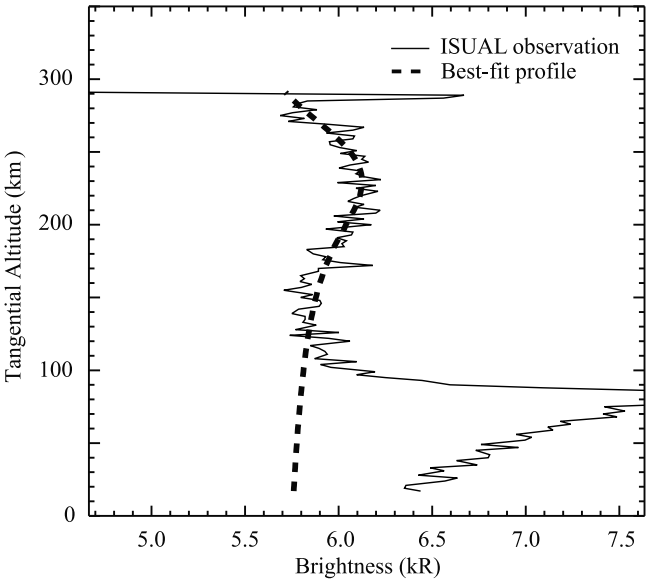

Figure 3. The apparent altitude profile of ISUAL-observed 630-nm airglow (solid line) and the best fit profile (dotted line) reproduced from the Gaussian assumption in Figure 4. The strong emission at around 80 km is the OH airglow layer, and we ignored this altitude range in producing best fit profiles of ISUAL-observed data.

order. Applying this analysis process to all the images, we derive the midnight altitude-latitude distributions of 630 nm airglow in the Asian sector.

3. Altitude-Latitude Characteristics of 630 nm Airglow at Midnight

[8] Figure 5 shows the relationship between the peak height z_p and the maximum intensity I_p of the 630 nm airglow. Figure 5 represents all the data ISUAL obtained from 14 days of observation during 2006–2008. Data points at lower-volume emission rates show significant scatter in altitude owing to analysis errors in the iteration process. Above ~230 km, we find a negative correlation between altitude and luminosity because rich molecular oxygen at lower altitudes produces stronger airglow emissions. A similar tendency was found by *Chandra et al.* [1973] using Ogo-4 photometric data. They found a negative correlation between the altitude of maximum emission rate and integrated emission intensity. The scale height H in the exponential luminosity distribution was 40–45 km in their study while that estimated from our data (Z_p > 230 km) was less than ~22 km. Because the negative correlation between luminosity and altitude is due primarily to the altitude profile of the O_2^+ density, we can assume that H derived from these two studies corresponds to the scale height of molecular oxygen. Thus, it is possible to estimate a neutral temperature from the relation of $H = k_B T/m(O_2)g$, where k_B is the Boltzmann constant, $m(O_2)$ is the mass of molecular oxygen, and g is the gravitational acceleration. *Chandra et al.* [1973] found that scale heights of 40–45 km correspond to neutral temperatures of 1200–1400°K which are typical values in the high solar-flux period. For H = 22 km in our study, the temperature is estimated to be ~830°K which is typical in the low solar-flux period. Since the airglow data of *Chandra et al.* [1973] were obtained in the solar maximum phase while our data were obtained in the solar minimum phase, the discrepancy in the scale heights of these two studies can be explained by the solar activity.

[9] Figure 6 shows the midnight altitude-latitude distributions of 630 nm airglow in the Asian sector observed on 20 and 21 December 2007. On these two nights, geomagnetic activity was relatively high (ΣKp = 26, 30+). We found that the locations of bright airglow regions were significantly different between the two nights. On the first night, we found two airglow regions: a bright region at 20°S–0° (30°S–10°S MLAT) and a somewhat weaker

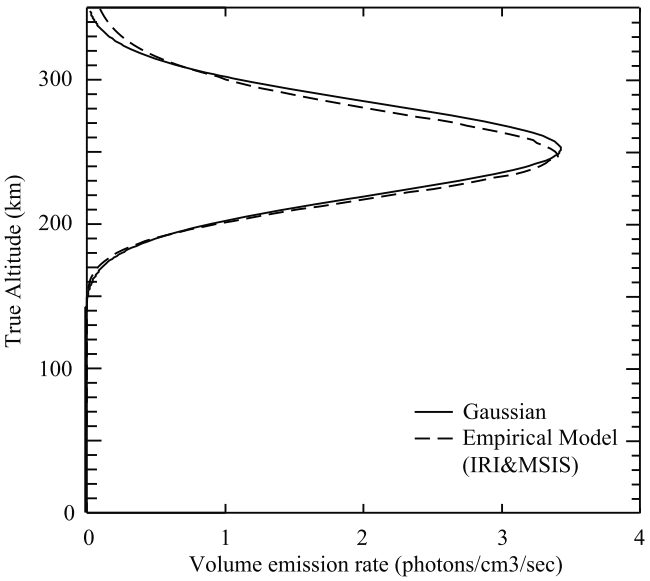

Figure 4. The true Gaussian altitude profile which best fits the ISUAL apparent profile in Figure 3 (solid line) and an empirical airglow distribution calculated from MSIS-E-90 and IRI models (dashed line).

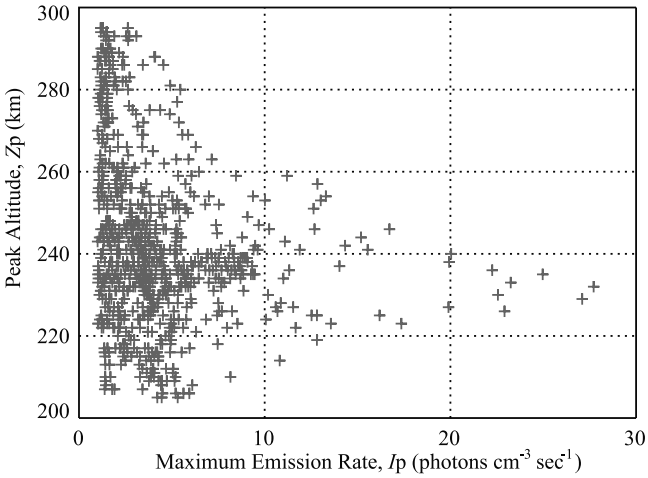

Figure 5. A scatterplot showing the relation between the peak altitude z_p and the maximum volume emission rate I_p. We produced one data point from each airglow snapshot. More than 100 data points obtained from a total of 14 days of observation are plotted.

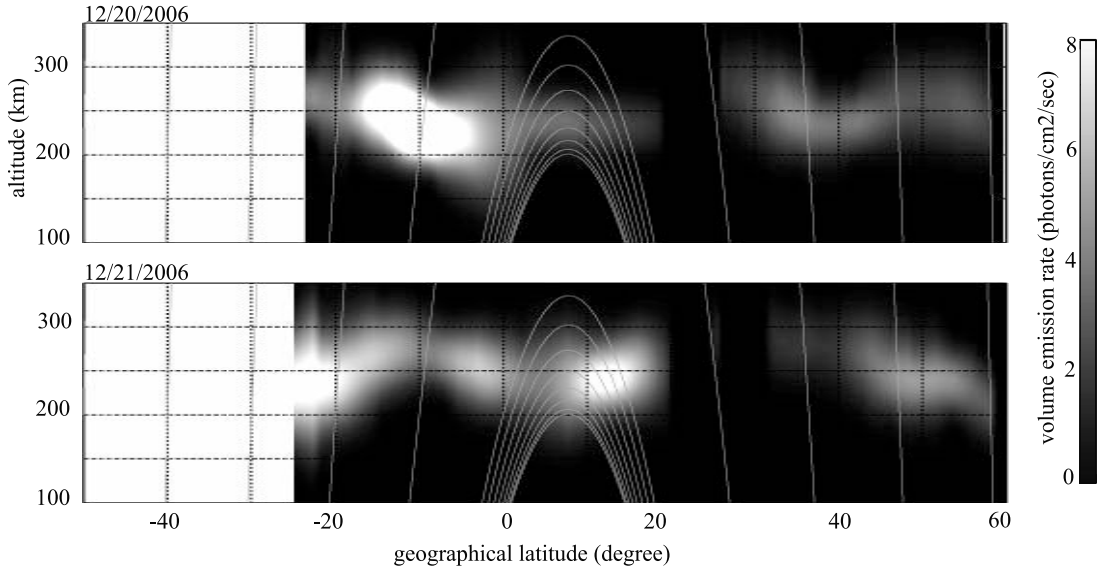

Figure 6. Midnight altitude-latitude airglow distributions obtained during the geomagnetic active phase. Also shown are magnetic field lines. The observation range is shifted to the winter hemisphere (Northern Hemisphere in this case).

region at 30°N–60°N (20°N–50°N MLAT). On the next night, four bright regions were visible at latitudes around 25°S–15°S, 7°S–0°, 8°N–20°N, and 40°N–60°N (35°S–25°S, 17°S–10°S, 0°–10°N, 30°N–50°N MLAT). Thus, it is clear that the number and locations of bright airglow regions are totally different between these two successive nights. Because such a feature was not found on quiet nights, the variability is probably related to the geomagnetic activity. The airglow behavior under high geomagnetic activity is an important issue which should be studied further in near future.

[10] On the remaining twelve nights in May–June 2007 and in April–May 2008, geomagnetic activity was relatively quiet (ΣKp = 4–20). Figure 7 represents the midnight altitude-latitude distributions of 630 nm airglow on these nights. In contrast to the disturbed conditions, we consistently found two stable airglow regions at midlatitudes (40°S–10°S) and around the equator (0°–5°N). It is interesting that both regions have different characteristics in terms of the spatial scale and brightness. The equatorial airglow was basically localized to the latitude range of 5°–10° while the midlatitude airglow regions were wider than 30°. In addition, night-to-night variation in brightness was also different between these two regions. For example, on 3–6 May 2008, the brightness of the midlatitude airglow was almost constant in the range of 4–6 photons cm^{-3} s^{-1} while that of the equatorial airglow was highly variable in the range of 4–15 photons cm^{-3} s^{-1}. These characteristics suggest that the generation processes of each airglow region are different.

[11] Past satellite measurements clarified the global distribution of 630 nm airglow. The Ogo-4 satellite observed tropical arcs that are asymmetrical with respect to the geomagnetic equator due to the north–south difference in the *F* region height. In the Asian sector, *Chandra et al.* [1973] found a bright airglow at 20°N–25°N (10°N–15°S MLAT) and a somewhat weaker airglow at 0°–5°S (10°S–15°S MLAT) at ~2200 LT in the semi equinox season. However, we note here that no bright airglow is found at the corresponding latitudes in Figure 7. The inconsistency between these two studies is probably due to the ~2 h difference in the local time. *Colerico et al.* [1996] found the premidnight brightness wave, which results from the decaying tropical arc, propagating equatorward over Arequipa in Peru (~5°S MLAT) at 2000–2200 LT. This finding suggests that the dissipation of the tropical arc occurs before the midnight. Therefore, it agrees well with the fact that *Chandra et al.* [1973] observed the tropical arc at ~2200 LT while we did not find it at ~0000 LT in the ISUAL measurements.

[12] Since ISUAL observes airglow at ~0000 LT, it is important to discuss the results in relation to the general behavior of the midnight *F* region ionosphere. Using both MSIS and IRI empirical models, we calculated typical airglow distributions at local midnight (not shown in the present paper). The results showed that the brightness of the airglow is maximized at 30°S–10°S (40°S–20°S MLAT) with intensities of 3–7 photons cm^{-3} s^{-1}. The optical emission intensity observed by ISUAL is also in the same range of 4–6 photons cm^{-3} s^{-1}. Furthermore, we find a zenith integration of ISUAL-observed airglow corresponds to 30–80 R, which is close to the typical luminosity of 50–100 R observed from the ground in the midlatitude region [e.g., *Otsuka et al.*, 2003]. As such, ISUAL-observed midlatitude airglow could be explained by elementary physical processes occurring in the *F* region ionosphere. In the nighttime, equatorward neutral winds flowing at *F* region altitudes move plasma upward along the magnetic line. Because the recombination rate decreases as the altitude increases, the plasma uplifted higher survives for a longer time. In this way, plasma created in the daytime remains until midnight and maintains the optical emissions of the nightglow. This effect is maximized at latitudes of 10°S–20°S (20°S–30°S MLAT) where the magnetic dip angle is about 45°, which is the best condition for the vertical motion

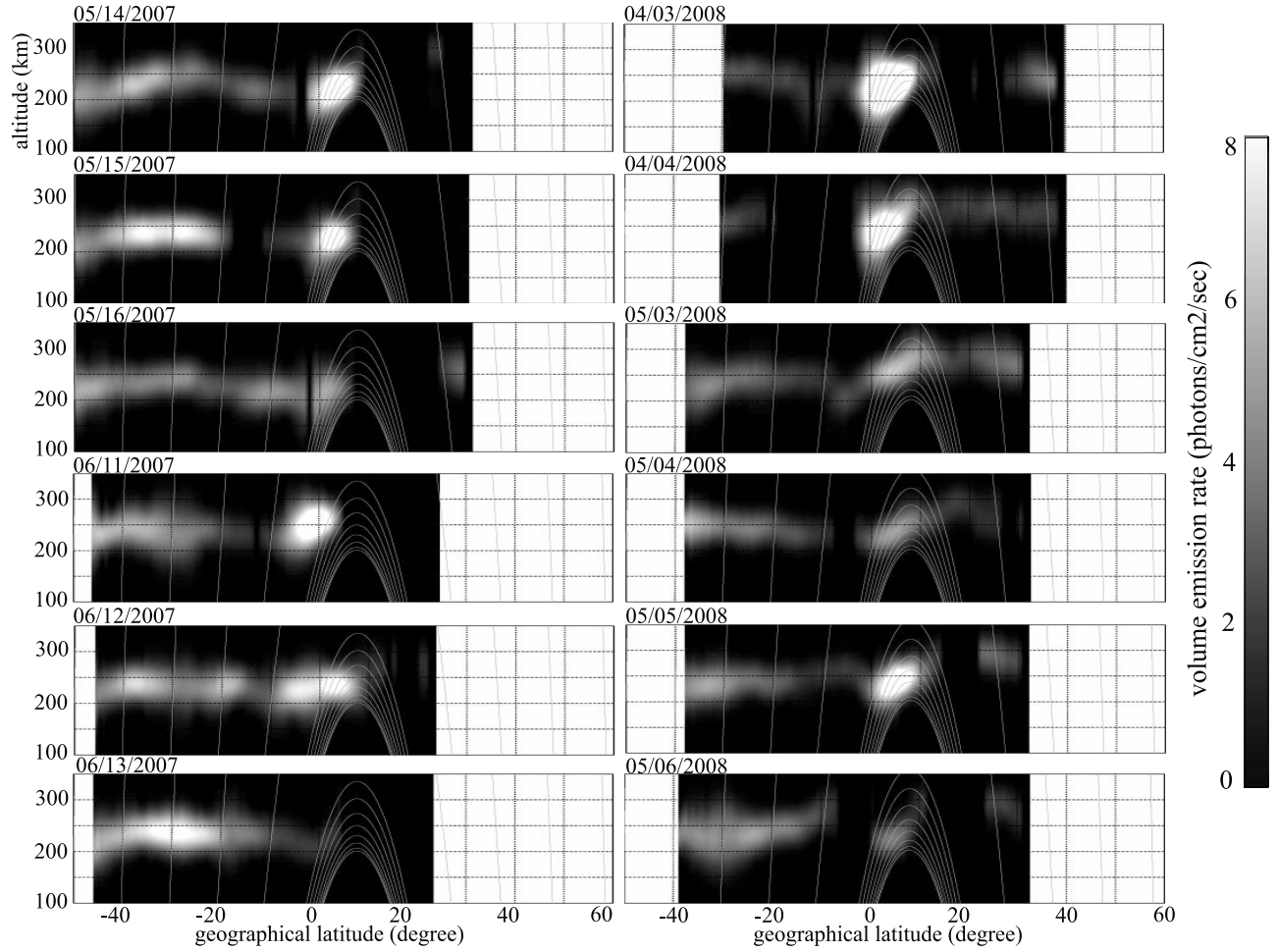

Figure 7. Same as Figure 6 but for midnight altitude-latitude airglow distributions obtained during the geomagnetic quiet phase.

of plasma by meridional winds. Consequently, the optical emission of airglow is strongest at midlatitudes. Although the daytime fountain effect transports plasma from the equator to low latitudes, the plasma density is effectively reduced by the recombination process because the *F* region plasma remains at lower altitudes. Therefore, optical emissions of airglow would not be discernible at the low-latitude region.

[13] In the equatorial region, it is known that bright airglow emissions are often observed around local midnight. *Greenspan* [1966] found a signature of bright airglow which is accompanied with the midnight temperature maximum (MTM) caused by the thermospheric wind system. Recent observational studies carried out in South America clarified two types of nighttime airglow occurring around the geographic equator: the premidnight brightness wave (PMBW) and the midnight brightness wave (MBW) [*Colerico et al.*, 1996]. PMBW is a somewhat fainter wave which propagates equatorward at 2000–2200 LT while MBW is a brighter wave which propagates poleward at 2300–0100 LT. Recent analysis by *Colerico et al.* [2006] explained PMBW as the decaying intertropical arcs. However, MBW is explained in relation to MTM which is produced in the perimeter of the equatorial pressure bulge formed by the convergence of tidal winds [e.g., *Meriwether et al.*, 2008]. Because ISUAL primarily observes the region around local midnight (~0000 LT), the equatorial airglow consistently found at 0°–10°N (10°S–0° MLAT) in Figure 7 corresponds to MBW and not to PMBW. Integrating the true altitude profile in the vertical direction, we found that ISUAL-observed tropical airglow is as bright as 224 R, which is consistent with the typical brightness (100–200 R) of MBW reported in past ground measurements [e.g., *Colerico et al.*, 1996]. One might find that the center of the equatorial airglow is somewhat offset from the geographical equator, but these offsets are within the ~5° error which comes from the observational geometry. Figure 8 shows two close-up images of the equatorial airglow observed on 14 May 2007 and 5 May 2008. The airglow structures are clearly curved along the magnetic field line, representing the electromagnetic behavior of the plasma. As discussed by *Meriwether et al.* [2008], MBW is due to the vertical transport of plasma driven by the thermospheric meridional wind. In the midnight sector, equatorward winds converge at around the equator and create a pressure bulge. The pressure bulge drives winds reversely to the poleward direction in its perimeter and transports plasma downward along the magnetic field line. Such a downward plasma motion in the midnight sector is also evident in other experimental studies using ionograms and radars and is known as the midnight

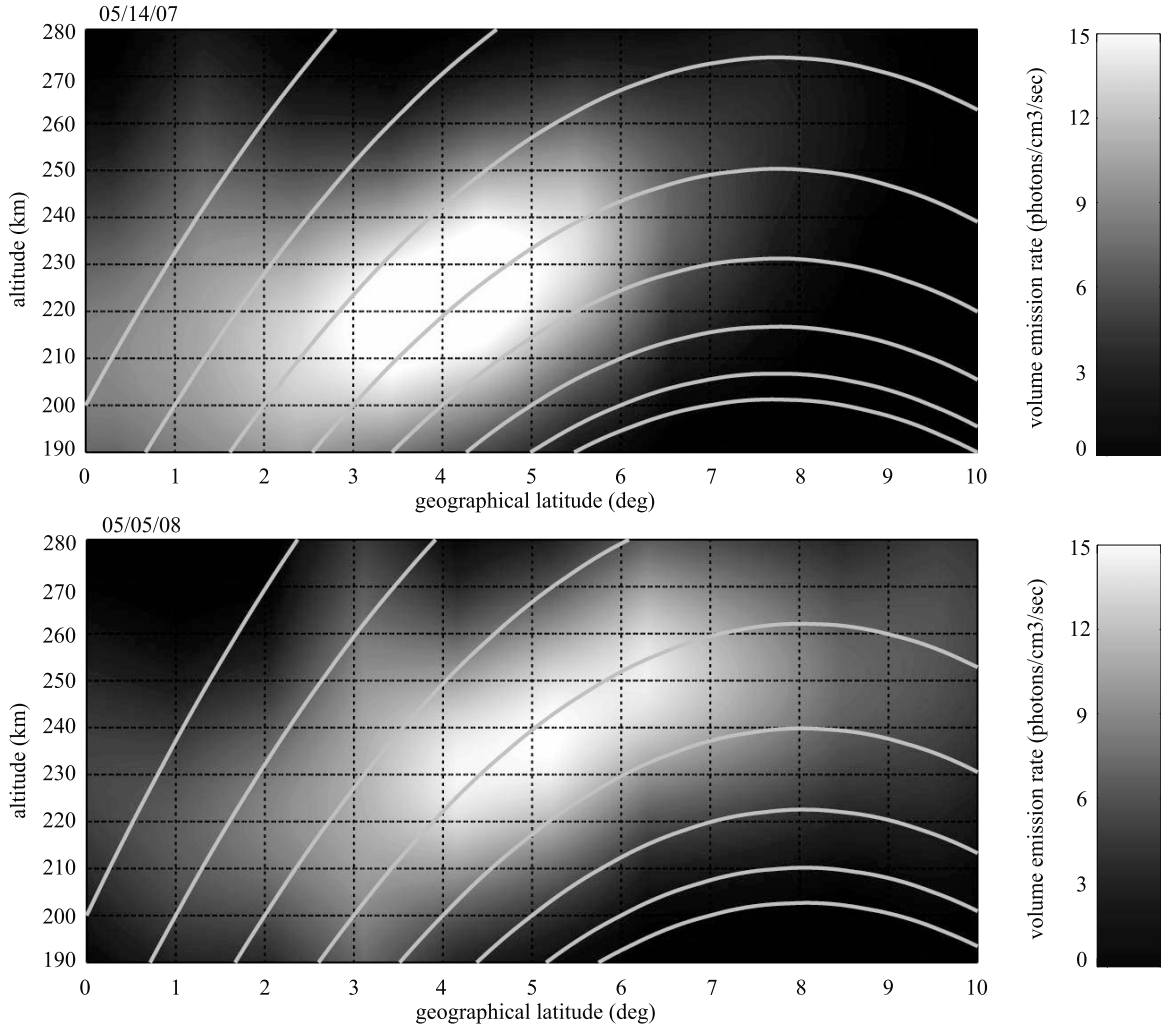

Figure 8. Close-up images of equatorial airglows in the quiet phase obtained on (top) 14 May 2007 and (bottom) 5 May 2008. Also shown are magnetic field lines.

collapse [e.g., *Nelson and Cogger* 1971; *Behnke and Harper*, 1973]. The field-aligned airglow structures found in this study might support the idea that the midnight vertical transport of plasma is the cause of MBW.

[14] It is interesting that the data obtained on 12 June 2007 (see Figure 9) represents two bright cores of airglow which were located to the north (0°–6°N) and to the south (7°S–1°S) of the geographic equator. This data might represent the cross section of two branches of a V-shaped MBW. Past experimental studies have clarified that MBW has a V-shape structure which branches at the midnight equator toward both northeast and southeast directions [*Meriwether et al.*, 2008]. Because the locations of MTM were found to be variable, the branch-point would sometimes be located at the east or at the west of local midnight. In the case of MTM with a branch-point located at midnight, ISUAL would detect only one bright core. But in the case of MTM with a branch-point located at premidnight, ISUAL would detect two bright cores corresponding to the cross section of the north and south branches (see Figure 9). However, in the case of MTM located at postmidnight, ISUAL would detect no bright core of airglow (see the data of 13 June 2007) because MBW is far beyond the detection coverage of ISUAL. In Figure 9, we also note that the north core is brighter than the south core. Because the north hemisphere corresponds to summer on this night, the feature is consistent with the fact that MTM is more pronounced in summer than in winter [*Herrero and Spencer*, 1982].

[15] It is worth discussing the north–south asymmetry in 630 nm airglow with respect to the magnetic equator. Since the observation coverage of ISUAL is shifted toward the winter hemisphere to avoid strong solar background noise in the summer hemisphere, we cannot discuss the symmetry/asymmetry of airglow in the whole latitude range. Even so, ISUAL clearly observed the conjugate region of the equatorial airglow. In Figure 7, we find no significant optical emissions in the latitude range of 10°N–20°N (0°–10°N MLAT) which is the conjugate region of the equatorial airglow. The brightness in the conjugate region is at least lower than the detectable threshold of ~0.4 photons cm^{-3} s^{-1}. Past research reported that intertropical arcs seen in 630 nm airglow could also be asymmetrical with respect to the magnetic equator because the global wind system controls the *F* region height. A recent study by *Lin et al.* [2007] confirmed the asymmetrical behavior of EIA on the basis of the FORMOSAT-3/COSMIC measurements. However, it should

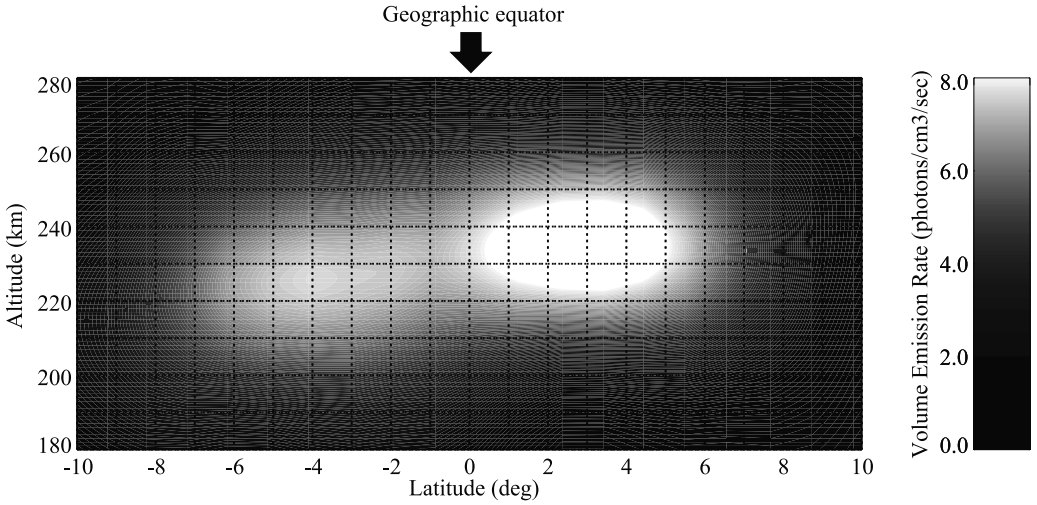

Figure 9. Close-up image of equatorial airglows on 12 June 2007. The two bright cores are symmetrically located with respect to the geographical equator rather than the geomagnetic equator (~8°N).

be noted again that we found no conjugate emissions with respect to the magnetic equator and instead found symmetrical emissions with respect to the geographical equator on 12 June 2007. These findings support the idea that the equatorial airglow found in the present study corresponds to MBW and not to EIA/PMBW.

4. Comparison With Plasma Measurements

[16] On 11 June 2008, two spacecrafts simultaneously observed the plasma density in the same area. During a period from 1425 to 1503 UT, the Langmuir probe on board the CHAMP satellite measured in situ the plasma density flying from 80°S to 80°N latitudes around ~135°E longitude. Details on the CHAMP satellite orbit and plasma density measurements can be found in the work of *Liu et al.* [2007]. FORMOSAT-3/COSMIC instrument simultaneously carried out plasma density measurement in a similar region using the occultation technique. Figure 10 represents comparisons between airglow and plasma distributions observed by these spacecrafts. We find a weak plasma enhancement in the southern midlatitude region (40°S–20°S) and a strong

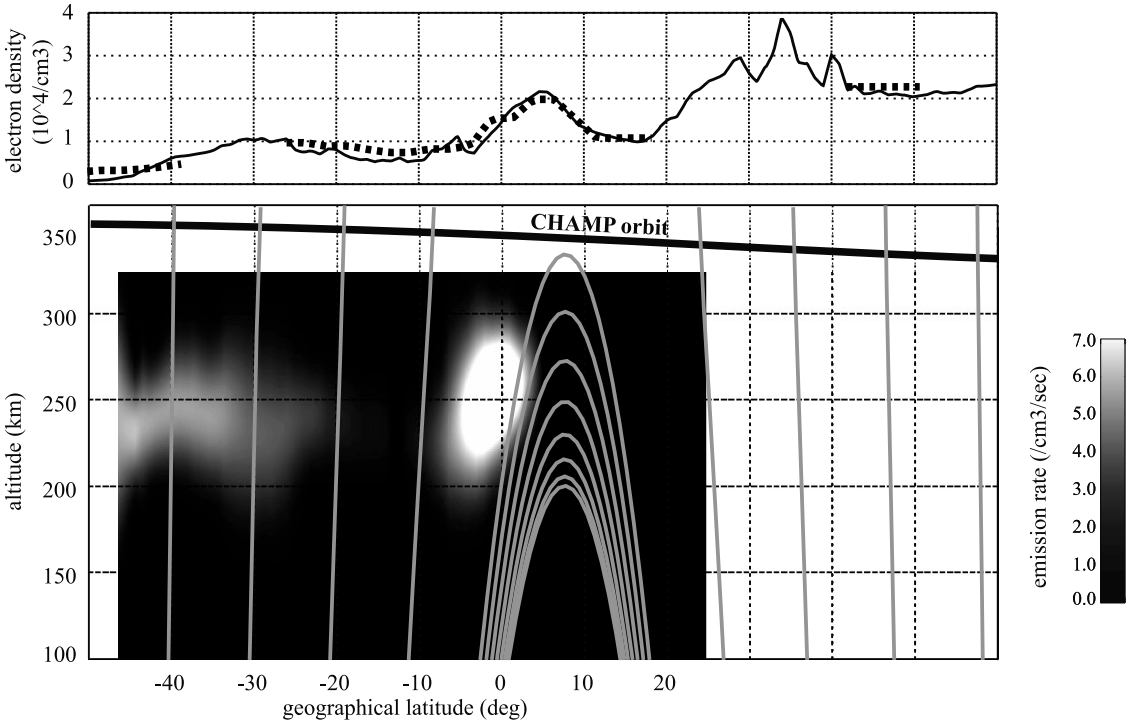

Figure 10. (top) Plasma densities observed by CHAMP (solid line) and FORMOSAT-3/COSMIC (dotted line). (bottom) ISUAL-observed airglow distribution on 11 June 2007. Also shown are magnetic field lines in gray solid lines and the orbit of the CHAMP satellite in a black solid line.

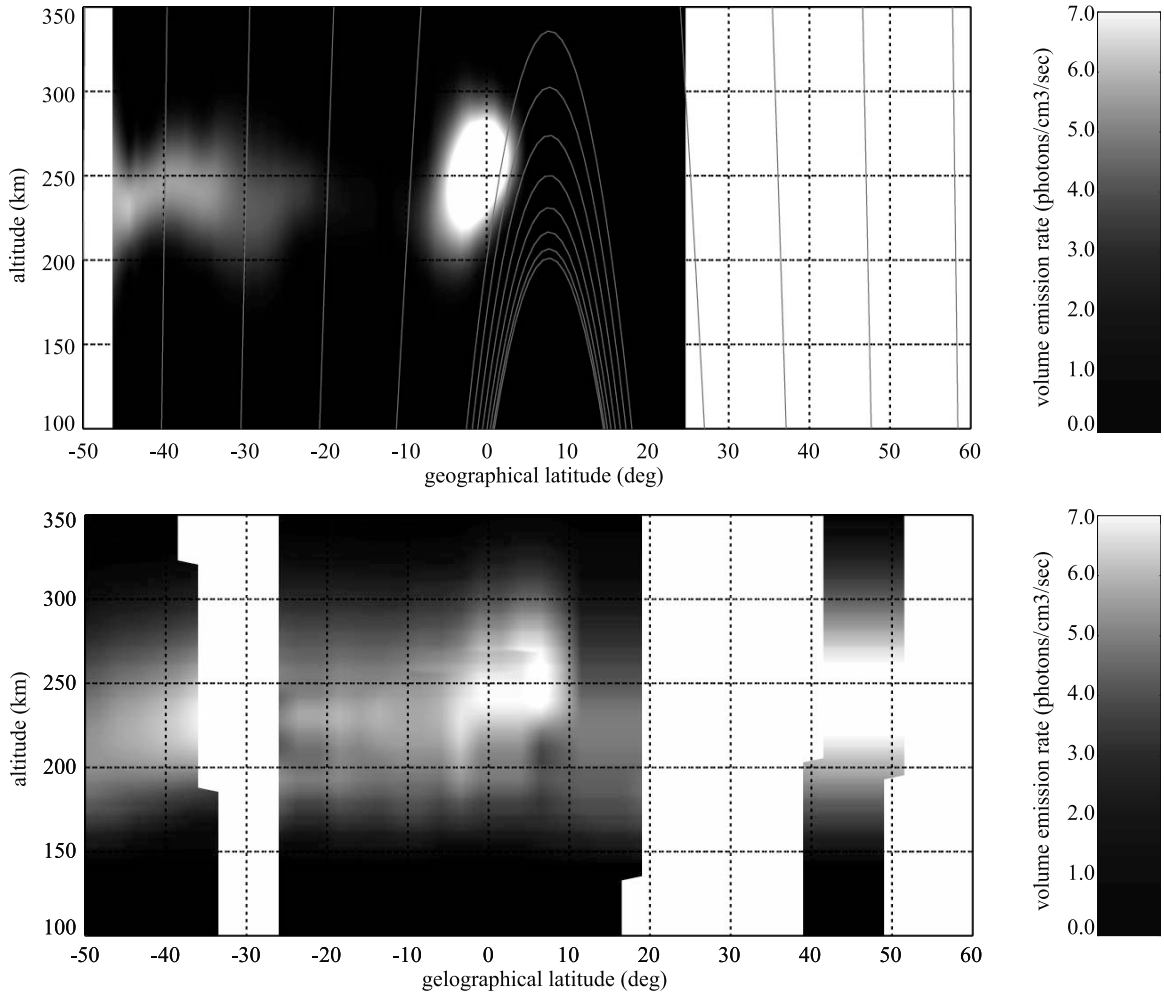

Figure 11. (top) ISUAL-observed airglow on 11 June 2007. (bottom) Airglow distribution calculated from COSMIC plasma data and the MSIS-E-90 model.

plasma enhancement in the equatorial region (0°S–10°N). Both of them are clearly located on the same magnetic field lines as the ISUAL-observed airglows at lower altitudes. We note here that the plasma density measured by COSMIC agrees well with that measured by CHAMP. The discrepancies between these two measurements are only $<0.2 \times 10^4$ cm^{-3}, which correspond to 10–20% differences at the equatorial region. The consistency between COSMIC and CHAMP measurements also suggests that the plasma structures discussed here had large spatial scales. This also justifies the comparisons with ISUAL measurements because ISUAL observes only large-scale airglow structure. Therefore, the plasma data used in this work is sufficiently accurate to discuss macroscopic structures in the *F* region ionosphere.

[17] Figure 11 shows a comparison between ISUAL and COSMIC data. Figure 11 (top) shows the airglow distribution calculated from the COSMIC-observed plasma distribution. As explained earlier, the intensity of the 630 nm airglow can be calculated from the neutral and electron densities using equation (4). Here, we use the electron density observed by COSMIC and the neutral density obtained from the MSIS-E-90 empirical model. Figure 11 (bottom) shows airglow distribution actually observed by ISUAL. We find two bright airglow regions in ISUAL data: one is at midlatitudes (47°S–22°S) and the other is around the geographic equator (8°S–4°N). Similarly, the airglow distributions calculated from COSMIC plasma data also indicate two bright regions at the midlatitudes (50°S–35°S) and at the equator (5°S–8°N). In the midlatitude region, both data have consistent emission intensities of 3–4 photons cm^{-3} s^{-1} which suggests that the brightness of airglow can be fully explained by the plasma density. However, in the case of the equatorial region, luminosities calculated from COSMIC data and those observed by ISUAL were ~5 and ~8 photons cm^{-3} s^{-1}, respectively. Because this difference is significantly larger than the ISUAL analysis error of ~1 photons cm^{-3} s^{-1}, we discuss the inconsistency in detail.

[18] One possible explanation is a small difference in the observational geometries between ISUAL and COSMIC. If these two satellites observe longitudinally uniform airglow, a small geometric discrepancy does not make such a large difference. But if the airglow has a nonuniform longitudinal structure, we can expect some discrepancies between these two measurements. Therefore, a significant discrepancy between COSMIC and ISUAL data might suggest a nonuniform structure of the equatorial airglow such as the V-shaped MBW. Because we find a good agreement in the midlatitudes, the airglow in this region would be longitu-

dinally uniform. Another possibility is the anomaly in neutral density accompanied with MTM. *Arduini et al.* [1997] and *Liu et al.* [2005] reported characteristics of the midnight density maximum (MDM) which is created during the production of MTM. Analyzing the data obtained from satellite in situ measurements, they found neutral density enhancements of a few to a few tens of percent at 0000–0200 LT. Assuming 50% enhancement in the density of molecular oxygen, the brightness of the airglow is increased by 50%. In Figure 11 (top), we used neutral data derived from MSIS-E-90 which does not reflect the MDM feature. Therefore, the discrepancy between COSMIC and ISUAL data might partly be due to a possible enhancement of neutral density such as MDM. No matter which explanation is right, the discrepancy in the equatorial region between ISUAL and COSMIC data can be explained as a consequence of MTM/MBW phenomena. Because the equatorial airglow was much brighter than the midlatitude airglow and was commonly seen in most nights, further extensive studies of the MTM/MBW phenomenology, which fails to be reproduced in the current general circulation model [e.g., *Fesen et al.*, 2002; *Colerico et al.*, 2006], are required.

5. Summary

[19] We correctly inferred the first true altitude profile of 630 nm airglow and derived its latitudinal structure in both hemispheres in the midnight Asian sector. The altitude of the peak luminosity was negatively correlated with the volume emission rate and was in good agreement with past observational and theoretical studies. The geomagnetic activity was found to have a strong influence on the latitude distribution of the airglow. In relatively active phases, the number and locations of bright airglows were totally different on successive nights. In relatively quiet phases, we found two bright airglows which were consistently located in the midlatitude and equatorial regions. Comparing ISUAL airglow data with CHAMP and COSMIC plasma data, we found plasma enhancements located on the same magnetic lines as the bright airglow regions. Quantitative analysis showed that the airglow in the equatorial region was due to the MBW produced in association with the MTM while that in the midlatitude airglow was consistent with the typical plasma distribution usually formed at local midnight. The fact that the bright equatorial airglow was commonly observed on most nights suggests a need to further study the MTM/MBW phenomenology, which is not accurately reproduced in the current general circulation model.

[20] **Acknowledgments.** T.A. and H.L. are supported by JSPS under Research Fellowships for Young Scientists. The contributions of R.R.H. and A.B.C.s are supported by research grant 93-NSPO(B)-ISUAL-FA09-01.

[21] Robert Lysak thanks John Meriwether and another reviewer for their assistance in evaluating this paper.

References

Abreu, V. J., G. A. Schmitt, P. B. Hays, and T. P. Dachev (1982), Volume emission rate profiles of the 6300-Å tropical nightglow obtained from the AE-E Satellite: Latitudinal and seasonal variations, *J. Geophys. Res.*, *87*, 6346–6352, doi:10.1029/JA087iA08p06346.

Adachi, T., et al. (2008), Electric fields and electron energies in sprites and temporal evolutions of lightning charge moment, *J. Phys. D Appl. Phys.*, *41*, 234010, doi:10.1088/0022-3727/41/23/234010.

Arduini, C., U. Ponzi, and G. Laneve (1997), Tidal analysis of the San Marco V and San Marco III: Density data in equatorial orbit, *J. Atmos. Sol. Terr. Phys.*, *59*, 1491–1503, doi:10.1016/S1364-6826(96)00151-4.

Barbier, D., and J. Glaume (1960), Les radiations de l'oxygène 6300 et 5577 Å de la luminescene du ciel nocturne dans une station de basse latitude, *Ann. Geophys.*, *16*, 319–334.

Behnke, R. A., and R. M. Harper (1973), Vector measurements of *F* region ion-transport at Arecibo, *J. Geophys. Res.*, *78*, 8222–8234, doi:10.1029/JA078i034p08222.

Bhatnagar, V. P., and G. G. Shepherd (1989), The seasonal-variations in the nighttime 6300- Å emission at midlatitudes from ISIS-II spacecraft, *J. Atmos. Terr. Phys.*, *51*, 11–12, 867–872, doi:10.1016/0021-9169(89)90003-2.

Blamont, J. E., J. M. Luton, and J. S. Nisbet (1974), Global temperature distributions from Ogo-6 6300 Å airglow measurements, *Radio Sci.*, *9*, 247–251, doi:10.1029/RS009i002p00247.

Burrage, M. D., C. G. Fesen, and V. J. Abreu (1990), Low-latitude thermospheric neutral winds determined from AE-E measurements of the 6300-Å nightglow at solar maximum, *J. Geophys. Res.*, *95*, 10,357–10,364, doi:10.1029/JA095iA07p10357.

Chandra, S., E. L. Reed, B. E. Troy, and J. E. Blamont (1973), Equatorial airglow and ionospheric geomagnetic anomaly, *J. Geophys. Res.*, *78*, 4630–4640, doi:10.1029/JA078i022p04630.

Chen, A. B., et al. (2008), Global distributions and occurrence rates of transient luminous events, *J. Geophys. Res.*, *113*, A08306, doi:10.1029/2008JA013101.

Chern, J. L., R. R. Hsu, H. T. Su, S. B. Mende, H. Fukunishi, Y. Takahashi, and L. C. Lee (2003), Global survey of upper atmospheric transient luminous events on the ROCSAT-2 satellite, *J. Atmos. Sol. Terr. Phys.*, *65*, 647–659, doi:10.1016/S1364-6826(02)00317-6.

Colerico, M., M. Mendillo, D. Nottingham, J. Baumgardner, J. Meriwether, J. Mirick, B. W. Reinisch, J. L. Scali, C. G. Fesen, and M. A. Biondi (1996), Coordinated measurements of *F* region dynamics related to the thermospheric midnight temperature maximum, *J. Geophys. Res.*, *101*, 26,783–26,793, doi:10.1029/96JA02337.

Colerico, M. J., M. Mendillo, C. G. Fesen, and J. Meriwether (2006), Comparative investigations of equatorial electrodynamics and low-to-mid latitude coupling of the thermospheric-ionosphere system, *Ann. Geophys.*, *24*, 503–513, doi:10.5194/angeo-24-503-2006.

Fesen, C. G., D. L. Hysell, J. W. Meriwether, M. Mendillo, B. G. Fejer, R. G. Roble, B. W. Reinisch, and M. A. Biondi (2002), Modeling of the low latitude thermosphere and ionosphere, *J. Atmos. Sol. Terr. Phys.*, *64*, 1337–1349.

Frey, S., S. B. Mende, and H. U. Frey (2001), Satellite limb tomography applied to airglow of the 630 nm emission, *J. Geophys. Res.*, *106*, 21,367–21,380, doi:10.1029/2001JA900024.

Greenspan, J. A. (1966), Synoptic description of 6300 Å nightglow near 78° west longitude, *J. Atmos. Terr. Phys.*, *28*, 739–745.

Herrero, F. A., and N. W. Spencer (1982), On the horizontal distribution of the equatorial thermospheric midnight temperature maximum and its seasonal variation, *Geophys. Res. Lett.*, *9*(10), 1179–1182, doi:10.1029/GL009i010p01179.

Lin, C. H., J. Y. Liu, T. W. Fang, P. Y. Chang, H. F. Tsai, C. H. Chen, and C. C. Hsiao (2007), Motions of the equatorial ionization anomaly crests imaged by FORMOSAT-3/COSMIC, *Geophys. Res. Lett.*, *34*, L19101, doi:10.1029/2007GL030741.

Liu, H., V. Henize, and W. Köhler (2005), Global distribution of the thermospheric total mass density derived from CHAMP, *J. Geophys. Res.*, *110*, A04301, doi:10.1029/2004JA010741.

Liu, H., C. Stolle, M. Förster, and S. Watanabe (2007), Solar activity dependence of the electron density in the equatorial anomaly regions observed by CHAMP, *J. Geophys. Res.*, *112*, A11311, doi:10.1029/2007JA012616.

Mende, S. B., G. R. Swenson, S. P. Geller, R. A. Viereck, E. Murad, and C. P. Pike (1993), Limb view spectrum of the Earth airglow, *J. Geophys. Res.*, *98*, 19,117–19,125, doi:10.1029/93JA02282.

Mende, S. B., H. U. Frey, R. R. Hsu, H. T. Su, A. B. Chen, L. C. Lee, D. D. Sentman, Y. Takahashi, and H. Fukunishi (2005), *D* region ionization by lightning-induced electromagnetic pulses, *J. Geophys. Res.*, *110*, A11312, doi:10.1029/2005JA011064.

Meriwether, J., M. Faivre, C. Fesen, P. Sherwood, and O. Veliz (2008), New results on equatorial thermospheric winds and the midnight temperature maximum, *Ann. Geophys.*, *26*, 447–466, doi:10.5194/angeo-26-447-2008.

Nelson, S. J., and L. L. Cogger (1971), Dynamical behavior of nighttime ionosphere at Arecibo, *J. Atmos. Terr. Phys.*, *33*, 1711–1726.

Nikoukar, R., G. R. Swenson, A. Z. Liu, and F. Kamalabadi (2007), On the variability of mesospheric OH emission profiles, *J. Geophys. Res.*, *112*, D19109, doi:10.1029/2007JD008601.

Otsuka, Y., T. Kadota, K. Shiokawa, T. Ogawa, S. Kawamura, S. Fukao, and S.-R. Zhang (2003), Optical and radio measurements of a 630-nm airglow enhancement over Japan on 9 September 1999, *J. Geophys. Res.*, *108*(A6), 1252, doi:10.1029/2002JA009594.

Otsuka, Y., K. Shiokawa, T. Ogawa, and P. Wilkinson (2004), Geomagnetic conjugate observations of medium-scale traveling ionospheric disturbances at midlatitude using all-sky airglow imagers, *Geophys. Res. Lett.*, *31*, L15803, doi:10.1029/2004GL020262.

Rajesh, P. K., et al. (2009), First results of the limb imaging of 630.0 nm airglow using FORMOSAT-2/Imager of Sprites and Upper Atmospheric Lightnings, *J. Geophys. Res.*, *114*, A10302, doi:10.1029/2009JA014087.

Reed, E. I., W. B. Fowler, and J. E. Blamont (1973), An atlas of low-latitude 6300-Å [OI] night airglow from Ogo 4 observations, *J. Geophys. Res.*, *78*, 5658–5675, doi:10.1029/JA078i025p05658.

Saito, A., et al. (2001), Traveling ionospheric disturbances detected in the FRONT campaign, *Geophys. Res. Lett.*, *28*, 689–692, doi:10.1029/2000GL011884.

Shiokawa, K., et al. (2003), Thermospheric wind during a storm-time large-scale traveling ionospheric disturbance, *J. Geophys. Res.*, *108*(A12), 1423, doi:10.1029/2003JA010001.

Sobral, J. H. A., H. Takahashi, M. A. Abdu, P. Muralikrishna, Y. Sahai, C. J. Zamlutti, E. R. de Paula, and P. P. Batista (1993), Determination of the quenching rate of the $O(^1D)$ by $O(^3D)$ from rocket-borne optical (630 nm) and electron density data, *J. Geophys. Res.*, *98*, 7791–7798, doi:10.1029/92JA01839.

Thuilleir, G., and J. E. Blamont (1973), Vertical red line 6300 Å distribution and tropical nightglow morphology in quiet magnetic conditions, in *Physics and Chemistry of Upper Atmospheres: Proceedings of a Symposium Organized by the Summer Advanced Study Institute, Held at the University of Orleans, France, July 31 to August 11, 1972*, edited by B. M. McCormac, pp. 219–231, D. Reidel, Boston, Mass.

Thuillier, G., R. H. Wiens, G. G. Shepherd, and R. G. Roble (2002), Photochemistry and dynamics in thermospheric intertropical arcs measured by the WIND Imaging Interferometer on board UARS: A comparison with TIE-GCM simulations, *J. Atmos. Sol. Terr. Phys.*, *64*, 405–415, doi:10.1016/S1364-6826(01)00109-2.

T. Adachi, STAR Laboratory, Stanford University, Packard Building Room 354, 350 Serra Mall, Stanford, CA 94305, USA. (tadachi@stanford.edu)

A. B. Chen and R.-R. Hsu, Department of Physics, National Cheng Kung University, Tainan 70701, Taiwan.

C.-C. Hsiao, National Space Organization, Prosperity 1st Road, Science-Based Industrial Park, Hsin-Chu, Taiwan.

H. Liu, M. Yamamoto, and M. Yamaoka, Research Institute for Sustainable Humanosphere, Kyoto University, Uji, Kyoto 611-0011, Japan.

Y. Otsuka, Solar-Terrestrial Environment Laboratory, Nagoya University, Furo-cho, Chikusa-ku, Nagoya 464-8601, Japan.